HHS Public Access

Author manuscript

Exp Eye Res. Author manuscript; available in PMC 2019 May 01.

Published in final edited form as:

Exp Eye Res. 2018 May ; 170: 177–187. doi:10.1016/j.exer.2018.02.018.

Fibrocyte migration, differentiation and apoptosis during the corneal wound healing response to injury

Luciana Lassance, PhD[1], **Gustavo K. Marino, MD, PhD**[2], **Carla S. Medeiros, MD**[1,2], **Shanmugapriya Thangavadivel, PhD**[1], and **Steven E. Wilson, MD**[1]

[1]Cole Eye Institute, Cleveland Clinic, Cleveland, Ohio

[2]University of Sao Paulo, Sao Paulo, Brazil

Abstract

The aim of this study was to determine whether bone marrow-derived fibrocytes migrate into the cornea after stromal scar-producing injury and differentiate into alpha-smooth muscle actin (αSMA) + myofibroblasts. Chimeric mice expressing green fluorescent protein (GFP) bone marrow cells had fibrosis (haze)-generating irregular phototherapeutic keratectomy (PTK). Multiplex immunohistochemistry (IHC) for GFP and fibrocyte markers (CD34, CD45, and vimentin) was used to detect fibrocyte infiltration into the corneal stroma and the development of GFP+ αSMA+ myofibroblasts. IHC for activated caspase-3, GFP and CD45 was used to detect fibrocyte and other hematopoietic cells undergoing apoptosis. Moderate haze developed in PTK-treated mouse corneas at 14 days after surgery and worsened, and persisted, at 21 days after surgery. GFP+CD34+CD45+ fibrocytes, likely in addition to other CD34+ and/or CD 45+ hematopoietic and stem/progenitor cells, infiltrated the cornea and were present in the stroma in high numbers by one day after PTK. The fibrocytes and other bone marrow-derived cells progressively decreased at four days and seven days after surgery. At four days after PTK, 5% of the GFP+ cells expressed activated caspase-3. At 14 days after PTK, more than 50% of GFP +CD45+ cells were also αSMA+ myofibroblasts. At 21 days after PTK, few GFP+αSMA+ cells persisted in the stroma and more than 95% of those remaining expressed activated caspase-3, indicating they were undergoing apoptosis. GFP+CD45+SMA+ cells that developed from 4 to 21 days after irregular PTK were likely developed from fibrocytes. After irregular PTK in the strain of C57BL/6—C57/BL/6-Tg(UBC-GFP)30Scha/J chimeric mice, however, more than 95% of fibrocytes and other hematopoietic cells underwent apoptosis prior to the development of mature αSMA+ myofibroblasts. Most GFP+CD45+αSMA+ myofibroblasts that did develop subsequently underwent apoptosis—likely due to epithelial basement membrane regeneration and deprivation of epithelium-derived TGFβ requisite for myofibroblast survival.

Corresponding Author: Steven E. Wilson, MD, Cole Eye Institute, I-32, Cleveland Clinic, 9500 Euclid Ave, Cleveland, OH, United States, wilsons4@ccf.org.

Proprietary interest statement

None of the authors have any commercial or proprietary interest in this study.

Keywords

fibrocytes; fibrosis; myofibroblasts; apoptosis; haze; cornea wound healing

1. Introduction

Fibrocytes are monocyte-derived mesenchymal cells that circulate as mononuclear cells in the peripheral blood and commonly differentiate into myofibroblasts to contribute to wound healing responses in many organs (Darby et al., 2014). These cells express CD45, a leukocyte marker, CD34 and CD11b, hematopoietic progenitor cell markers, chemokine receptors such as chemokine (C–C motif) receptor (CCR) 3, CCR5, CCR7 and chemokine (C-X-C motif) receptor (CXCR) 4 and extracellular matrix molecules such as collagens type I, fibronectin and vimentin (Reilkoff, Bucala and Herzog, 2011). Fibrocytes rapidly infiltrate sites of injury and participate in healing and remodeling of the affected tissues (Abe et al., 2001; Chesney et al., 1998), but they may also contribute to pathological fibrosis (Reilkoff, Bucala and Herzog, 2011). Fibrocytes have been identified in fibrotic tissues in a variety of diseases such as lung fibrosis, bronchopulmonary dysplasia, liver fibrosis, renal fibrosis and scars in skin (Ashley et al., 2017; Iwaisako et al., 2014; Karin et al., 2016; Li et al., 2016; Suda et al., 2016; Sun et al., 2016).

The development of fibrosis is associated with similar triggering events in different organs. These initiators include damage to the epithelial, endothelial, or parenchymal cells of the affected tissues and release of fibrogenic cytokines like transforming growth factor-β (TGF-β), recruitment of bone marrow-derived cells and the development of myofibroblasts that produce disordered extracellular matrix (Guarino et al., 2009; Krieg et al., 2007; Leaf and Duffield, 2017; Maher et al., 2007; Strutz and Muller, 1999). Myofibroblasts are characterized by the expression of α-smooth muscle actin (α-SMA), often with co-expression of vimentin and/or desmin (Chaurasia et al., 2009), contractility, and the secretion of extracellular matrix proteins such as fibronectin, collagen type I and collagen type III (Kaneda et al., 2017; Krieg et al., 2007).

Myofibroblast development and persistence after epithelial-stromal injury in the cornea commonly leads to stromal fibrosis and decreased corneal transparency (also referred to as haze or scarring) that compromises the ability of the cornea to transmit light (Jester et al., 1999c; Mohan et al., 2003; Wilson, 2012). The anterior corneal wound healing response triggered by trauma, infections, or corneal surgeries initiates a cascade of events that includes the release and penetration of TGF-β and platelet-derived growth factor (PDGF) into the stroma through the damaged epithelial basement membrane (EBM) that triggers myofibroblast development and may lead to persistence if repair of the EBM is delayed (Jester et al., 1999c; Torricelli et al., 2013a; Torricelli et al., 2013b). Myofibroblasts are opaque due to diminished crystallin protein production (Jester et al., 1999b), and they produce disorganized extracellular matrix that disrupts the precise distribution and spacing of the collagen fibers necessary for corneal transparency (Marino et al., 2017a; Marino et al., 2016).

Fibrocytes have been shown to be progenitors of myofibroblasts in fibrotic tissues in many organs (Abe et al., 2001; Direkze et al., 2003; Loomis-King and Moore, 2013; Xu et al., 2015), although myofibroblasts may also develop from local tissue fibroblasts (Gallego-Munoz et al., 2017; LeBleu et al., 2013; Tandon et al., 2010; Torricelli and Wilson, 2014; Wang et al., 2017) or, possibly, by epithelial-to-mesenchymal transition (EMT) where epithelial cells acquire a mesenchymal phenotype and develop into myofibroblasts (Sun et al., 2016). It has been demonstrated that myofibroblasts can develop in the cornea from keratocyte progeny, or even epithelial cells in some models (Direkze et al., 2003; Fathke et al., 2004; Saika et al., 2010; Wilson, 2012). However, bone marrow-derived cells that infiltrate the corneal stroma after injury have also been shown to differentiate into myofibroblasts in chimeric mice that express green fluorescent protein (GFP) in bone marrow-derived cells (Barbosa et al., 2010; Singh et al., 2013). The purpose of this study was to determine whether bone marrow-derived cells that give rise to myofibroblasts are fibrocytes and, if so, to study the timing of fibrocyte recruitment, differentiation into mature myofibroblasts, and death by apoptosis in the cornea after fibrosis-associated injury (Mohan et al., 2008).

2. Material and Methods

2.1 Animals, Chimerization and Generation of Corneal Fibrosis

All animals were treated in accordance with the tenets of the ARVO Statement for the Use of Animals in Ophthalmic and Vision Research and of the National Institutes of Health guide for care and use of laboratory animals. All experiments were approved by the Institutional Animal Care and Use Committee (IACUC) at the Cleveland Clinic. C57BL/6 (Stock Number: 000664) and C57BL/6-Tg(UBC-GFP)30Scha/J (Stock Number: 004353) female mice were obtained from The Jackson Laboratory (Bar Harbor, ME). These transgenic mice express enhanced green fluorescent protein (GFP) under the direction of the human ubiqutin C promoter in all tissues. Anesthesia was performed with an intraperitoneal injection of 130 mg ketamine and 8.8 mg xylazine per gram of body weight and 1 drop of 1% proparacaine HCl (Alcon, Ft., TX, USA) applied topically to the eye prior to phototherapeutic keratectomy (PTK). Ciprofloxacin hydrochloride 0.3% (Alcon) was instilled into the eye immediately after the procedure and continued twice a day until the epithelium was healed. Euthanasia was performed with an inhaled overdose of 5% isoflurane gas.

2.2 Bone Marrow Transplant for Generation of GFP Chimeric Mice

The GFP chimeric mice were generated using a previously described method (Barbosa et al., 2010; Singh et al., 2013). In brief, the tibia and femur of C57/BL/6-Tg(UBC-GFP)30Scha/J mice were removed after euthanasia and maintained in chilled 1X PBS (10X stock is 1.37M sodium chloride, 27mM potassium chloride, and 119mM phosphate buffer, endotoxin free) throughout the procedure. Care was taken to include the joints at both ends of the femur and tibia in each leg. Soft tissues and skin were removed, and the femur and tibia separated at the knee joint by dissecting the adjoining connective tissue. Both ends of the bones were trimmed to allow insertion of a 26-gauge needle to flush the bone marrow with DMEM medium. Importantly, tissue populated with bone marrow cells is found concentrated at the

joints. Bone marrow cells were harvested by flushing medium and scratching the bone marrow cavity with the end of the needle. Bone marrow cells were collected in a petri dish and clumps of bone marrow cells were teased out and gently dissociated using a one ml pipette to form a single-cell suspension. The suspension of cells was centrifuged at 1500 rpm for 10 minutes at 4°C to obtain a cell pellet. Red blood cells were lysed by adding sterile Milli-Q water at 4° C, followed by dilution with 10X PBS at 4°C at a ratio of one part PBS to nine parts cell solution with immediate mixing. Cell suspensions were centrifuged again at 1500 rpm for 10 minutes at 4°C and re-suspended in 1x PBS at 4°C. Cell viability in the range of 90% to 95% was verified by staining with 0.4% trypan blue and cells were suspended in PBS at 4°C at a final concentration of 20×10^6 cells/ml.

Recipient C57BL/6 wild type mice received gentamycin 5mg/kg by intraperitoneal injection two days prior to and 7 days after irradiation. The recipient animals were irradiated two hours before bone marrow transplant using a ^{137}Cs Mark 1 irradiator (J.L. Sheperd & Associates, Glendale, CA). All recipient mice received a single 600 rads dose of whole-body irradiation and were then allowed to rest in cages with unlimited food and water for two hours prior to bone marrow injection. Irradiated mice were placed briefly under an infrared lamp to allow dilation of the tail veins and were then immobilized using an animal holder and the tail vein located. The tails were sterilized using 70% ethanol pads and 0.5 ml of bone marrow cell suspension (20×10^6 cells/ml) was injected intravenously using a 30-gauge needle. Animal mortality was observed within one to two weeks if viable bone marrow cells were not delivered in adequate numbers.

A proportion of five GFP+ donors to six recipient wild type mice was used in this study to generate sufficient GFP+ chimeric mice expressing more than 90% GFP+ cells in the blood verified with fluorescence-activated cell sorting as previously described (Barbosa et al., 2010; Singh et al., 2013). This procedure reconstitutes the thymus, spleen, bone marrow and peripheral blood of the recipient mice with GFP+ bone marrow-derived cells.

Haze-generating irregular phototherapeutic keratectomy (PTK) with a fine mesh screen was performed on one eye of each chimeric GFP animal with a VISX S4IR excimer laser (Abbott Laboratories, Irvine, CA) as previously reported (Mohan et al., 2008), at two months after bone marrow transplantation, once chimerization of at least 90% was verified. The opposite eye of each animal served as a control.

2.3 Slit Lamp Analysis and Cornea Tissue Preparation

Groups of three animals each (triplicates) had slit lamp photos of corneal haze under general anesthesia, followed by euthanasia and eye removal and fixation at 1, 4, 7, 14 and 21 days after irregular PTK surgery. The experimental and control eyes were removed with 0.12 mm forceps and sharp Westcott scissors, embedded in liquid OCT compound (Sakura Fine Tek, Torrance, CA, USA) within a 15 mm × 15 mm × 5 mm mold (Fisher Scientific, Pittsburgh, PA, USA) and snap frozen using previously reported methods (Mohan et al., 2003). The frozen tissue blocks were maintained at 85°C until tissue sections were prepared. Tissue sections (8 micrometer thick) were cut with a cryostat (HM525, Thermo Scientific) and maintained frozen at 85°C until IHC was performed.

2.4 Multiplex Immunohistochemistry

Triple-immunohistochemistry (IHC) was performed on experimental and control corneal sections to study expression of GFP, CD34 and CD45, or GFP, vimentin and alpha-smooth muscle actin (αSMA) at each time point. Corneal sections were prepared from all animals in each time point. The grouping of antigens in multiplex IHC was dictated by available primary antibodies. Briefly, slides containing three or four sections of each eye were washed twice in 1xPBS for five minutes and then fixed using 4% paraformaldehyde for only five minutes. Slides were then washed twice in 1X PBS for 5 minutes and sections were blocked using 5% normal donkey serum (#017000121, Jackson Laboratories, ME, USA) in 1X PBS for 30 minutes at room temperature. Primaries antibodies diluted in 5% normal donkey serum in 1X PBS, in the combinations described above, were placed on the slides and incubated at room temperature for one hour. Dilutions of primary antibodies were as follows: chicken anti-GFP antibody (ab13870, Abcam, Cambridge, UK) was diluted 1:2000, rat anti-CD45 antibody (MCD455, Thermo Fisher, MA, USA), sheep anti-CD34 (AF6518, R&D Systems, MN, USA) and rabbit anti-αSMA (ab5694, Abcam) were diluted 1:100 and the goat anti-vimentin (sc-7557, Santa Cruz, TX, USA) was diluted 1:50. After primary antibody incubation, slides were washed twice in 1X PBS for 5 minutes and secondary antibodies, also diluted in 5% normal donkey serum in 1X PBS, were added to the sections for one hour at room temperature as follows: Combination 1: donkey anti-chicken Alexa fluor 488 (#703-545-155, Jackson Immuno Research, PA, USA) at 1:500 + donkey anti-sheep Alexa fluor 647 (A-21448, Thermo Fisher) at 1:200 + donkey anti-rat Alexa fluor 594 (A-21209, Thermo Fisher) at 1:500; used for triple staining GFP, CD34 and CD45. Combination 2: donkey anti-chicken Alexa fluor 488 at 1:500 + donkey anti-rabbit Alexa fluor 568 (A-10042, Thermo Fisher) at 1:200 + donkey anti-goat Alexa fluor 647 (A-21447, Thermo Fisher) 1:200; used for triple staining GFP, αSMA and vimentin. Slides were finally washed three times in 1X PBS, air dried and mounted with Vectashield mounting media containing DAPI (H-1200, Vector Laboratories, CA, USA) to allow visualization of all nuclei. Sections for negative controls were included with incubations with secondary antibodies alone in the same dilutions as described above. The sections were analyzed and photographed with a Leica DM5000 microscope (Leica, Buffalo Grove, IL) equipped with Q-imaging Retiga 4000RV (Surrey, BC, Canada) camera and Image-Pro software (MediaCybernetics, Inc. Bethesda, MD).

Immunohistochemistry for collagen type 1 was performed using primary antibody goat anti-type I collagen (catalog #1310-01, Southern Biotech, Birmingham, AL USA) at a concentration of 1:500 to 1:5000 and secondary antibody donkey anti-goat IgG Alexa Fluor 594 (catalog # A11058, Thermo Fisher Scientific, Waltham, MA, USA) at a concentration of 1:200. Intense stromal staining for collagen type 1, however, precluded evaluation of infiltrating cells that were collagen type 1+ (Supplement Fig. 2).

Cells that presented positive staining for each combination of multiplex were manually counted in at least 3 sections per slide for each animal analyzed. Counts of marker-stained and apoptotic cells were determined in 400X stromal fields, utilizing several fields on three slides within the central cornea for each unwounded control and wounded cornea. The mean

and standard deviation of the marker-stained or apoptotic fields of three corneas at each time point were determined.

The non-parametric Kruskal-Wallis test was used to compare the wounded groups to the unwounded control group and a $p<0.01$ was considered statistically significant due to the large number of statistical comparisons performed.

2.5 Immunohistochemistry for Detection of Apoptotic Cells

Triple-IHC staining was performed on experimental and control tissue sections to study apoptosis by looking at the co-expression of cleaved caspase-3, GFP and CD45 in cornea sections of each time point. IHC was performed as described in the prior section. The antibody to cleaved caspase-3 (#9661S, Cell Signaling, MA, USA) was diluted 1:200 in 5% normal donkey serum in 1X PBS in combination with chicken anti-GFP protein and rat anti-CD45 in the dilutions previously described. Donkey anti-rabbit alexa fluor 568 was used as the secondary antibody in the dilution 1:500 in combination with donkey anti-chicken alexa fluor 488 (1:500) and donkey anti-rat alexa fluor 647 (1:200, ab150155, Abcam).

3. Results

3.1 Slit-lamp Evaluation of Haze Formation

Slit lamp photographs of the corneas of each animal revealed no visible corneal haze at 1, 4 or 7 days after PTK (Fig 1B, 1C and 1D), and were not different from control eyes without PTK (Fig. 1A). Mild spotty corneal haze was observed in all six eyes observed at 14 days after PTK (Fig. 1 E). Dense geographic haze was present in all three eyes observed at 21 days after PTK (Fig. 1F).

3.2 Fibrocyte Migration into the Cornea

Multiplex IHC in control unwounded corneas (Fig. 2) detected no GFP+ bone marrow-derived cells in the stroma. A few cells in control unwounded corneas, likely including resident macrophages, were CD45+ and/or CD34+. Many keratocytes also express vimentin, albeit at low levels.

In corneas at one day post PTK (Fig. 3, Table 1), there were large numbers of GFP+ cells (arrows) in the stroma of chimeric mice, indicating that bone marrow-derived cells migrated into the corneas. Most of these cells were also CD45+ (arrows) and CD34+ (arrows) but αSMA-. Approximately 23% of these GFP+/αSMA- cells were also vimentin+, which likely includes fibrocytes that infiltrated the stroma by one day after PTK. CD34+CD45+ cells that are vimentin- are likely other hematopoietic and hematopoietic stem/progenitor cells.

3.3 Fibrocytes and other hematopoietic cells accumulate in the cornea

At 4 days (Fig. 4, Table 1) after PTK, multiplex IHC showed there were large numbers of GFP+ cells (arrows) in the stroma of chimeric mice. Most of these GFP+ cells were also CD45+ (arrows) and CD34+ (arrows, in the overlay), indicating invading hematopoietic cells. Approximately 24% of the GFP+ cells also expressed vimentin which includes

fibrocytes, although other vimentin+ cells could also be present. At this early time point after PTK, only one αSMA+ cell (arrow, myofibroblast) was detected in one cornea and this cell was GFP+ indicating it had differentiated from bone marrow-derived cells.

At 7 days after PTK in chimeric mice (not shown), there remained many GFP+ stromal cells in the stroma and most of these cells were also CD45+ and CD34+. Two or three αSMA+ cells were found in each corneal section analyzed and more than 90% of these myofibroblasts were also GFP+.

3.4 Ongoing myofibroblast development in the stroma

At 14 days after PTK in chimeric mice (Fig. 5, Table 1), GFP+ (arrows), CD45+ (arrows) and CD34+ (arrows) cells, including some co-expressing all three markers (seen in the lower left overlay, arrows) were present in the stroma, but the density of these cells was decreased compared to 4 days (Fig. 4) and 7 days after PTK. At this time point (Fig. 5), most GFP+ cells co-expressed αSMA and vimentin (arrows in overlay bottom right) and approximately two to three times more αSMA+ cells were present in each corneal section of all three corneas compared 7 days after PTK. Also, at this time point, 30 to 50% of αSMA+ cells in each corneal section were GFP- (arrowheads), indicating these myofibroblasts likely differentiated from local keratocyte progeny.

At 21 days after PTK in chimeric mice (Fig. 6), fewer GFP+, CD45+, and CD34+ cells, including cells expressing all three markers (overlay bottom left), were present in the stroma. All GFP+ cells observed in all three corneas were αSMA+, confirming the bone marrow-derived fibrocyte origin of these cells. Approximately 30 to 50% of αSMA+ myofibroblasts were GFP-, indicating keratocytes were likely the progenitors for these myofibroblasts. There was a notable decrease in the total density of αSMA+ myofibroblasts in corneas at day 21 after PTK compared to corneas at day 14 after PTK.

3.5 Apoptosis in Bone Marrow-derived Cells, including Fibrocytes, after PTK

There were no cells expressing cleaved caspase-3 in the stroma of unwounded control corneas or at 1 day after PTK, except in the corneal epithelium (data not shown). One to three cleaved caspase-3-positive cells were present per section in the stroma at 4 days after PTK in all cornea sections analyzed and more than 95% of these cells were also GFP+ and CD45+ (not shown). At 7, 14, and 21 days after PTK in chimeric mice (Fig. 7, Table 2) between two and four cleaved caspase-3 expressing stromal cells were detected in each corneal section and more than 95% of these cells were also GFP+ and CD45+ (arrows, including in the overlays). Thus, many bone marrow-derived cells, including fibrocytes, that invade the corneal stroma after irregular PTK undergo apoptosis by 4 days and later after surgery.

4. Discussion

This study investigated whether bone marrow-derived fibrocytes migrate to the cornea after fibrosis-generating epithelial-stromal injury and develop into αSMA+ myofibroblasts, which generate the corneal fibrosis (scarring or haze). Prior studies in GFP chimeric mice confirmed the importance of bone marrow-derived cells (BMDC) in the generation of

fibrosis with 30 to 70% of persisting myofibroblasts originating from BMDC, with the rest derived from keratocytes, in a particular animal (Barbosa et al., 2010; Singh et al., 2013).

Mice are relatively resistant to generation of fibrosis after surface injuries like photorefractive keratectomy (PRK) compared to rabbits (Mohan et al., 2003; Torricelli et al., 2013a; Torricelli et al., 2013b) and humans (Torricelli et al., 2016), and irregular phototherapeutic keratectomy over a fine mesh screen must be used to roughen the stromal surface to mechanically inhibit epithelial basement membrane (EBM) regeneration in this species (Mohan, et al., 2008). The resistance to stromal fibrosis generation in mice is thought to be related to their proficiency in repairing the injured EBM (Marino et al., 2016; Torricelli et al., 2013a; Torricelli et al., 2013b) and, therefore, halting epithelial-derived TGFβ penetration into the stroma, and thereby triggering apoptosis of TGFβ-dependent myofibroblast precursors and mature myofibroblasts (Marino, et al, 2017a and 2017b). Prior studies demonstrated that the development of fibrosis (haze) after irregular PTK is dependent on mouse strain (Singh, et al., 2013). The C57BL/6 strain used in this study, because of the availability C57BL/6 GFP donors, is in the middle of the range of fibrotic tendency in mice and, therefore, it was expected that many myofibroblast precursor cells would undergo apoptosis during their development—which was confirmed in this study.

The present study demonstrated that many of the BMDC that invade the stroma after stromal-epithelial injury express CD34 and CD45 markers characteristic of fibrocytes (Reilkoff, Bucala and Herzog, 2011), although other hematopoietic lineage cells (Nakano, et al., 1990), including possibly other CD34+ hematopoietic stem/progenitor cells (Holyoake and Alcorn, 1994), are likely also infiltrating the corneal stroma. Many of these invading BMDC also expressed vimentin, which is characteristic of fibrocytes (Reilkoff, Bucala and Herzog, 2011) and, therefore, invading fibrocytes are likely among this population of cells. What can be deduced conclusively from the present study is that the GFP+/CD45+/αSMA+ cells noted in the stroma from 4 to 21 days after irregular PTK are developing corneal myofibroblasts (GFP+vimentin+αSMA+desmin-) or fully matured corneal myofibroblasts (GFP+vimentin+αSMA+desmin+) that developed from bone marrow-derived cells that were fibrocytes, although desmin expression was not studied.

Keratocytes also express low levels of vimentin (Chaurasia et al., 2009; Xu et al., 2008), but they would be GFP-CD34-CD45-αSMA- cells. Small numbers of GFP- CD34+ CD45+ cells were detected in the stroma of unwounded control corneas (Fig. 2) and these were likely resident macrophages and myeloid precursor cells (Brissette-Storkus et al., 2002; Sosnova et al., 2005). GFP+CD34+CD45+ cells that are vimentin- are other types of BMDC, including macrophages and other inflammatory cells. Importantly, fibrocytes often lose CD34 expression in later stages of their development into myofibroblasts (Diaz-Flores et al., 2014).

Rare GFP+ BMDC developed into SMA+ myofibroblasts as early as 4 days after irregular PTK (Fig. 4, Table 1), with no αSMA+ cells (either GFP+ or GFP-) being detected in the stroma of unwounded control corneas or corneas at one day after irregular PTK. Greater numbers of GFP+αSMA+ myofibroblasts were noted in the anterior stroma at 14 days (Fig. 5, Table 1) and 21 days (Fig. 6, Table 1) after PTK, but the numbers of these developing (or

mature) myofibroblasts was likely less than 1 to 2% of the total fibrocytes migrating into the corneal stroma at one day and later after PTK.

It would have been very useful to trace collagen type 1 in this study, as another important marker of fibrocytes (Bucala, et al,, 1994). However, cornea contains approximately 70% collagen type 1 (Newsome, Gross and Hassell, 1982; Newsome, et al., 1981) and IHC for collagen type 1 (Supplement Fig. 2) was so intense in all corneas tested that it precluded tracking of individual collagen type 1+ infiltrating cells.

In the present study, relatively few GFP+CD34+CD45+vimentin+ fibrocytes that invaded the cornea in the first few days after irregular PTK developed into mature GFP+CD45+SMA + myofibroblasts. IHC for activated cleaved caspase-3 (Fig. 7) demonstrated that most of the GFP+ CD45+ cells invading the cornea, including fibrocytes and their progeny, underwent apoptosis during the interval from 7 to 21 days after PTK. This apoptosis of GFP+CD45+ cells, including hematopoietic cells that were not fibrocytes, was detected as early as 4 days after the injury and would likely have been noted earlier if other time points between one day and four days had been included in this study. These fibrocytes that invade the cornea begin development into myofibroblasts, as do keratocyte-derived myofibroblast precursors, driven by high stromal levels of TGFβ (Jester et al., 1999a; Jester et al., 2002; Singh et al., 2014; Singh et al., 2011), and other cytokines such as PDGF (Jester et al., 2002; Singh et al., 2014), that penetrate the stroma from the injured epithelium and tear film in the first few days after injury before the epithelial basement membrane regenerates (Torricelli et al., 2016; Torricelli et al., 2013a; Torricelli et al., 2013b; Torricelli and Wilson, 2014). If the epithelial basement membrane regenerates through the coordinated action of epithelial and stromal cells (Torricelli et al., 2016; Wilson et al., 2017), stromal levels of TGFβ, and possibly other cytokines, decrease. Once they are deprived of this ongoing adequate supply of TGFβ, fibrocytes, fibrocyte progeny, and myofibroblasts (in addition to keratocyte progeny undergoing development into myofibroblasts) undergo apoptosis. If the injury is more extensive, yields a more irregular stromal surface, and/or is ongoing, and the epithelial basement membrane doesn’t regenerate, then fibrocyte and keratocyte-derived myofibroblast precursors complete their development into mature vimentin+αSMA+desmin+ myofibroblasts that produce fibrosis that persists—at least until the epithelial basement membrane is regenerated (Marino et al., 2017a and b). In the current experiments in mice, it is likely that epithelial basement membrane regeneration was sufficiently rapid, at least in some areas of the irregular PTK-ablated zone, so that myofibroblast development was abrogated prior to the appearance of many mature vimentin+αSMA+desmin+ myofibroblasts and relatively few areas of dense fibrosis emerged (Fig. 1) compared to what is seen in rabbits.

Fibrocytes have been found to have a role in myofibroblast generation and fibrosis in most organs investigated, including heart (Sopel et al., 2012), lung (Gurczynski et al., 2016), and skin (Abe et al., 2001; Kao et al., 2011), and liver (Iwaisako et al., 2012). Thus, although fibrocytes are only 0.1–0.5% of non-erythrocytic cells in the peripheral blood (Bucala et al., 1994), they make important contributions to the response to injuries throughout the body. In addition to myofibroblast development from local fibroblastic cells (keratocytes in the cornea), myofibroblasts can also develop by epithelial-to-mesenchymal transition (EMT), in

which epithelial cells acquire a mesenchymal phenotype and can give rise to fully-differentiated myofibroblasts (Iwaisako et al., 2012). Thus, myofibroblasts arise in injured tissues by at least three mechanisms, pointing to the importance of these cells to the viability of tissues and animals after injury. There is a temptation to think of fibrosis as only a pathological process. However, it clearly has an important function in the viability of organs and organisms, and only becomes pathological when it progresses and persists to the extreme where tissue repair is no longer possible. The cornea provides an excellent example of this principle. When the cornea develops overwhelming infection with pseudomonas aeruginosa bacteria, massive myofibroblast generation and fibrosis can prevent perforation of the cornea and loss of the eye (Marino et al., 2017a). Subsequently, over a period of months, after regeneration of the epithelial basement membrane, the myofibroblasts disappear, disordered extracellular matrix is reorganized, and transparency and visual function can be restored. This principle likely holds in all organs.

In summary, the present study demonstrates that fibrocytes contribute to corneal wound healing after epithelial-stroma injury in mice, by rapidly migrating to the site of injury and differentiating into mature αSMA-expressing myofibroblasts. It also confirms that the cornea has mechanisms in place to modulate the development of fibrocytes to mature myofibroblasts so that the latter cells are only generated in large numbers when they are needed.

Supplementary Material

Refer to Web version on PubMed Central for supplementary material.

Acknowledgments

Funding

Supported in part by US Public Health Service grants RO1EY10056 (SEW) and P30-EY025585 from the National Eye Institute, National Institutes of Health, Bethesda, MD and Research to Prevent Blindness, New York, NY. Dr. Lassance is supported by NEI training grant T32 EY007157.

The authors acknowledge the assistance of the Cleveland Clinic Lerner Research Institute Imaging Core in providing support with the immunohistochemistry multiplexing protocols and microscopy and the courtesy of the Flow Cytometry Core for acquiring flow cytometry data with the Becton-Dickinson LSR II.

References

Abe R, Donnelly SC, Peng T, Bucala R, Metz CN. Peripheral blood fibrocytes: differentiation pathway and migration to wound sites. J Immunol. 2001; 166:7556–7562. [PubMed: 11390511]

Ashley SL, Wilke CA, Kim KK, Moore BB. Periostin regulates fibrocyte function to promote myofibroblast differentiation and lung fibrosis. Mucosal Immunol. 2017; 10:341–351. [PubMed: 27435108]

Barbosa FL, Chaurasia SS, Cutler A, Asosingh K, Kaur H, de Medeiros FW, Agrawal V, Wilson SE. Corneal myofibroblast generation from bone marrow-derived cells. Exp Eye Res. 2010; 91:92–96. [PubMed: 20417632]

Brissette-Storkus CS, Reynolds SM, Lepisto AJ, Hendricks RL. Identification of a novel macrophage population in the normal mouse corneal stroma. Invest Ophthalmol Vis Sci. 2002; 43:2264–2271. [PubMed: 12091426]

Bucala R, Spiegel LA, Chesney J, Hogan M, Cerami A. Circulating fibrocytes define a new leukocyte subpopulation that mediates tissue repair. Mol Med. 1994; 1:71–81. [PubMed: 8790603]

Chaurasia SS, Kaur H, de Medeiros FW, Smith SD, Wilson SE. Dynamics of the expression of intermediate filaments vimentin and desmin during myofibroblast differentiation after corneal injury. Exp Eye Res. 2009; 89:133–139. [PubMed: 19285070]

Chesney J, Metz C, Stavitsky AB, Bacher M, RB. Regulated production of type I collagen and inflammatory cytokines by peripheral blood fibrocytes. J Immunol. 1998; 160:419–425. [PubMed: 9551999]

Darby IA, Laverdet B, Bonte F, Desmouliere A. Fibroblasts and myofibroblasts in wound healing. Clin Cosmet Investigat Dermatol. 2014; 7:301–311.

Diaz-Flores L, Gutierrez R, Garcia MP, Saez FJ, Diaz-Flores L Jr, Valladares F, Madrid JF. CD34+ stromal cells/fibroblasts/fibrocytes/telocytes as a tissue reserve and a principal source of mesenchymal cells. Location, morphology, function and role in pathology. Histol Histopathol. 2014; 29:831–870. [PubMed: 24488810]

Direkze NC, Forbes SJ, Brittan M, Hunt T, Jeffery R, Preston SL, Poulsom R, Hodivala-Dilke K, Alison MR, Wright NA. Multiple organ engraftment by bone-marrow-derived myofibroblasts and fibroblasts in bone-marrow-transplanted mice. Stem Cells. 2003; 21:514–520. [PubMed: 12968105]

Fathke C, Wilson L, Hutter J, Kapoor V, Smith A, Hocking A, Isik F. Contribution of bone marrow–derived cells to skin- collagen deposition and wound repair. Stem Cells. 2004; 22:812–822. [PubMed: 15342945]

Gallego-Munoz P, Ibares-Frias L, Valsero-Blanco MC, Cantalapiedra-Rodriguez R, Merayo-Lloves J, Martinez-Garcia MC. Effects of TGFbeta1, PDGF-BB, and bFGF, on human corneal fibroblasts proliferation and differentiation during stromal repair. Cytokine. 2017; 96:94–101. [PubMed: 28390267]

Guarino M, Tosoni A, Nebuloni M. Direct contribution of epithelium to organ fibrosis: epithelial-mesenchymal transition. Hum Pathol. 2009; 40:1365–1376. [PubMed: 19695676]

Gurczynski SJ, Procario MC, O'Dwyer DN, Wilke CA, Moore BB. Loss of CCR2 signaling alters leukocyte recruitment and exacerbates gamma-herpesvirus-induced pneumonitis and fibrosis following bone marrow transplantation. Am J Physiol Lung Cell Mol Physiol. 2016; 311:L611–627. [PubMed: 27448666]

Holyoake TL, Alcorn MJ. CD34+ positive haemopoietic cells: biology and clinical applications. Blood Rev. 1994; 8:113–24. [PubMed: 7524841]

Iwaisako K, Brenner DA, Kisseleva T. What's new in liver fibrosis? The origin of myofibroblasts in liver fibrosis. J Gastroenterol Hepatol. 2012; 27(Suppl 2):65–68. [PubMed: 22320919]

Iwaisako K, Jiang C, Zhang M, Cong M, Moore-Morris TJ, Park TJ, Liu X, Xu J, Wang P, Paik YH, Meng F, Asagiri M, Murray LA, Hofmann AF, Iida T, Glass CK, Brenner DA, Kisseleva T. Origin of myofibroblasts in the fibrotic liver in mice. Proc Natl Acad Sci USA. 2014; 111:E3297–3305. [PubMed: 25074909]

Jester JV, Huang J, Barry-Lane PA, Kao WW, Petroll WM, Cavanagh HD. Transforming growth factor(beta)-mediated corneal myofibroblast differentiation requires actin and fibronectin assembly. Invest Ophthalmol Vis Sci. 1999a; 40:1959–1967. [PubMed: 10440249]

Jester JV, Huang J, Petroll WM, Cavanagh HD. TGFbeta induced myofibroblast differentiation of rabbit keratocytes requires synergistic TGFbeta, PDGF and integrin signaling. Exp Eye Res. 2002; 75:645–657. [PubMed: 12470966]

Jester JV, Moller-Pedersen T, Huang J, Sax CM, Kays WT, Cavangh HD, Petroll WM, Piatigorsky J. The cellular basis of corneal transparency: evidence for 'corneal crystallins'. J Cell Sci. 1999b; 112(Pt 5):613–622. [PubMed: 9973596]

Jester JV, Petroll WM, Cavanagh HD. Corneal stromal wound healing in refractive surgery: the role of myofibroblasts. Prog Ret Eye Res. 1999c; 18:311–356.

Kaneda MM, Messer KS, Ralainirina N, Li H, Leem CJ, Gorjestani S, Woo G, Nguyen AV, Figueiredo CC, Foubert P, Schmid MC, Pink M, Winkler DG, Rausch M, Palombella VJ, Kutok J, McGovern K, Frazer KA, Wu X, Karin M, Sasik R, Cohen EE, Varner JA. Corrigendum: PI3Kgamma is a molecular switch that controls immune suppression. Nature. 2017; 542:124.

Kao HK, Chen B, Murphy GF, Li Q, Orgill DP, Guo L. Peripheral blood fibrocytes: enhancement of wound healing by cell proliferation, re-epithelialization, contraction, and angiogenesis. Ann Surg. 2011; 254:1066–1074. [PubMed: 21832942]

Karin D, Koyama Y, Brenner D, Kisseleva T. The characteristics of activated portal fibroblasts/myofibroblasts in liver fibrosis. Differentiation. 2016; 92:84–92. [PubMed: 27591095]

Krieg T, Abraham D, Lafyatis R. Fibrosis in connective tissue disease: the role of the myofibroblast and fibroblast-epithelial cell interactions. Arthritis Res Ther. 2007; 9:S4.

Leaf IA, Duffield JS. What can target kidney fibrosis? Nephrol Dial Transplant. 2017; 32:i89–i97. [PubMed: 28391346]

LeBleu VS, Taduri G, O'Connell J, Teng Y, Cooke VG, Woda C, Sugimoto H, Kalluri R. Origin and function of myofibroblasts in kidney fibrosis. Nat Med. 2013; 19:1047–1053. [PubMed: 23817022]

Li C, Li X, Deng C, Guo C. Circulating fibrocytes are increased in neonates with bronchopulmonary dysplasia. PloS One. 2016; 11:e0157181. [PubMed: 27309347]

Loomis-King H, Moore BB. Fibrocytes in the pathogenesis of chronic fibrotic lung disease. Curr Respir Med Rev. 2013; 9:34–41. [PubMed: 27512347]

Maher TM, Wells AU, Laurent GJ. Idiopathic pulmonary fibrosis: multiple causes and multiple mechanisms? Eur Respir J. 2007; 30:835–839. [PubMed: 17978154]

Marino GK, Santhiago MR, Santhanam A, Lassance L, Thangavadivel S, Medeiros CS, Bose K, Tam KP, Wilson SE. Epithelial basement membrane injury and regeneration modulates corneal fibrosis after pseudomonas corneal ulcers in rabbits. Exp Eye Res. 2017a; 161:101–105. [PubMed: 28506643]

Marino GK, Santhiago MR, Santhanam A, Torricelli AAM, Wilson SE. Regeneration of defective epithelial basement membrane and restoration of corneal transparency after photorefractive keratectomy. J Refract Surg. 2017b; 33:337–346. [PubMed: 28486725]

Marino GK, Santhiago MR, Torricelli AA, Santhanam A, Wilson SE. Corneal molecular and cellular biology for the refractive surgeon: the critical role of the epithelial basement membrane. J Refract Surg. 2016; 32:118–125. [PubMed: 26856429]

Mohan RR, Hutcheon AE, Choi R, Hong J, Lee J, Mohan RR, Ambrosio R Jr, Zieske JD, Wilson SE. Apoptosis, necrosis, proliferation, and myofibroblast generation in the stroma following LASIK and PRK. Exp Eye Res. 2003; 76:71–87. [PubMed: 12589777]

Mohan RR, Stapleton WM, Sinha S, Netto MV, Wilson SE. A novel method for generating corneal haze in anterior stroma of the mouse eye with the excimer laser. Exp Eye Res. 2008; 86:235–240. [PubMed: 18068702]

Nakano A, Harada T, Morikawa S, Kato Y. Expression of leukocyte common antigen (CD45) on various human leukemia/lymphoma cell lines. Acta Pathol Jpn. 1990; 40:107–15. [PubMed: 2140233]

Newsome DA, Foidart JM, Hassell JR, Krachmer JH, Rodrigues MM, Katz SI. Detection of specific collagen types in normal and keratoconus corneas. Invest Ophthalmol Vis Sci. 1981; 20:738–750. [PubMed: 7016805]

Newsome DA, Gross J, Hassell JR. Human corneal stroma contains three distinct collagens. Invest Ophthalmol Vis Sci. 1982; 22:376–381. [PubMed: 6277819]

Reilkoff RA, Bucala R, Herzog EL. Fibrocytes: emerging effector cells in chronic inflammation. Nat Rev Immunol. 2011; 11:427–435. [PubMed: 21597472]

Saika S, Yamanaka O, Sumioka T, Okada Y, Miyamoto T, Shirai K, Kitano A, Tanaka S. Transforming growth factor beta signal transduction: a potential target for maintenance/restoration of transparency of the cornea. Eye Contact Lens. 2010; 36:286–289. [PubMed: 20823707]

Singh V, Jaini R, Torricelli AA, Santhiago MR, Singh N, Ambati BK, Wilson SE. TGF beta and PDGF-B signaling blockade inhibits myofibroblast development from both bone marrow-derived and keratocyte-derived precursor cells in vivo. Exp Eye Res. 2014; 121:35–40. [PubMed: 24582892]

Singh V, Jaini R, Torricelli AA, Tuohy VK, Wilson SE. A method to generate enhanced GFP+ chimeric mice to study the role of bone marrow-derived cells in the eye. Exp Eye Res. 2013; 116:366–370. [PubMed: 24140502]

Singh V, Santhiago MR, Barbosa FL, Agrawal V, Singh N, Ambati BK, Wilson SE. Effect of TGF beta and PDGF-B blockade on corneal myofibroblast development in mice. Exp Eye Res. 2011; 93:810–817. [PubMed: 21978952]

Singh V, Torricelli AAM, Nayeb-Hashemi N, Agrawal V, Wilson SE. Mouse strain variation in SMA+ myofibroblast development after corneal injury. Exp Eye Res. 2013; 115:27–30. [PubMed: 23791965]

Sopel M, Falkenham A, Oxner A, Ma I, Lee TD, Legare JF. Fibroblast progenitor cells are recruited into the myocardium prior to the development of myocardial fibrosis. Int J Exp Pathol. 2012; 93:115–124. [PubMed: 22225615]

Sosnova M, Bradl M, Forrester JV. CD34+ corneal stromal cells are bone marrow-derived and express hemopoietic stem cell markers. Stem Cells. 2005; 23:507–515. [PubMed: 15790772]

Strutz F, Muller GA. Interstitial pathomechanisms underlying progressive tubulointerstitial damage. Kidney Blood Press Res. 1999; 22:71–80. [PubMed: 10352410]

Suda S, Williams H, Medbury HJ, Holland AJ. A review of monocytes and monocyte-derived cells in hypertrophic scarring post burn. J Burn Care Res. 2016; 37:265–272. [PubMed: 27003739]

Sun YB, Qu X, Caruana G, Li J. The origin of renal fibroblasts/myofibroblasts and the signals that trigger fibrosis. Differentiation. 2016; 92:102–107. [PubMed: 27262400]

Tandon A, Tovey JC, Sharma A, Gupta R, Mohan RR. Role of transforming growth factor Beta in corneal function, biology and pathology. Curr Mol Med. 2010; 10:565–578. [PubMed: 20642439]

Torricelli AA, Santhanam A, Wu J, Singh V, Wilson SE. The corneal fibrosis response to epithelial-stromal injury. Exp Eye Res. 2016; 142:110–118. [PubMed: 26675407]

Torricelli AA, Singh V, Agrawal V, Santhiago MR, Wilson SE. Transmission electron microscopy analysis of epithelial basement membrane repair in rabbit corneas with haze. Invest Ophthalmol Vis Sci. 2013a; 54:4026–4033. [PubMed: 23696606]

Torricelli AA, Singh V, Santhiago MR, Wilson SE. The corneal epithelial basement membrane: structure, function, and disease. Invest Ophthalmol Vis Sci. 2013b; 54:6390–6400. [PubMed: 24078382]

Torricelli AA, Wilson SE. Cellular and extracellular matrix modulation of corneal stromal opacity. Exp Eye Res. 2014; 129:151–160. [PubMed: 25281830]

Wang Q, Wang J, Wang J, Hong S, Han F, Chen J, Chen G. HMGB1 induces lung fibroblast to myofibroblast differentiation through NFkappaB mediated TGFbeta1 release. Mol Med Rep. 2017; 15:3062–3068. [PubMed: 28339089]

Wilson SE. Corneal myofibroblast biology and pathobiology: generation, persistence, and transparency. Exp Eye Res. 2012; 99:78–88. [PubMed: 22542905]

Wilson SE, Marino GK, Torricelli AAM, Medeiros CS. Injury and defective regeneration of the epithelial basement membrane in corneal fibrosis: A paradigm for fibrosis in other organs? Matrix Biol. 2017; 17:30141–5.

Xu J, Cong M, Park TJ, Scholten D, Brenner DA, Kisseleva T. Contribution of bone marrow-derived fibrocytes to liver fibrosis. Hepatobiliary Surg Nutr. 2015; 4:34–47. [PubMed: 25713803]

Xu Y, Xu Y, Huang C, Feng Y, Li Y, Wang W. Development of a rabbit corneal equivalent using an acellular corneal matrix of a porcine substrate. Mol Vis. 2008:2180–2189. [PubMed: 19052652]

Highlights

- Bone marrow-derived fibrocytes migrated to the cornea as early as 1 day after injury
- Fibrocytes began to differentiate into αSMA+ myofibroblasts
- Fibrocyte-derived myofibroblasts develop in parallel to keratocyte-derived myofibroblasts after injury
- Myofibroblast precursors undergo apoptosis if the epithelial basement membrane regenerates.

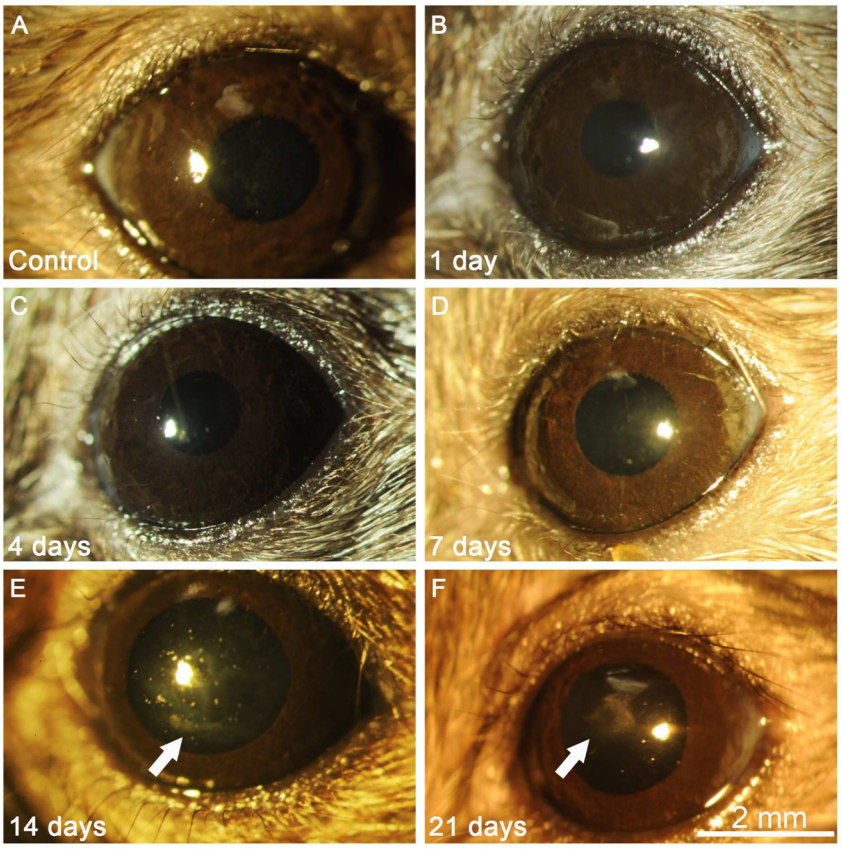

Fig. 1.

Slit lamp photos of unwounded control corneas and corneas one day after phototherapeutic keratectomy (PTK) in chimeric mice. (A) Control corneas were clear without opacity. Corneas at 1 day (B), 4 days (C) or 7 days (D) after PTK were also transparent. Mild spotty opacity restricted to the area of excimer laser ablation was noted in corneas (E, arrow) at 14 days after PTK (arrow). More dense but geographic subepithelial haze was present (F, arrow) at 21 days after PTK in all corneas. 25X mag.

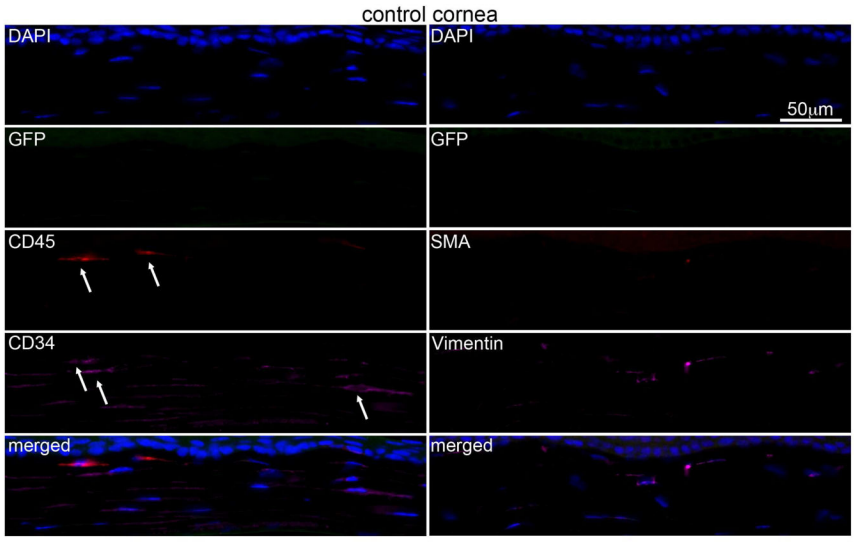

Fig. 2.

Multiplex immunohistochemistry (IHC) in the chimeric unwounded control mouse corneas. No visible bone marrow derived GFP or αSMA positive cells were detected in any unwounded control corneas. Few CD45+ (arrows) and/or CD34+ (arrows) cells were present in control corneas and these cells were GFP-negative. Blue is DAPI staining of cell nuclei and the merged panel is an overlay of all the images in that column. Negative control IHC was performed for all antigens without primary antibody and no staining was detected (see supplementary Fig. S1). 400x mag.

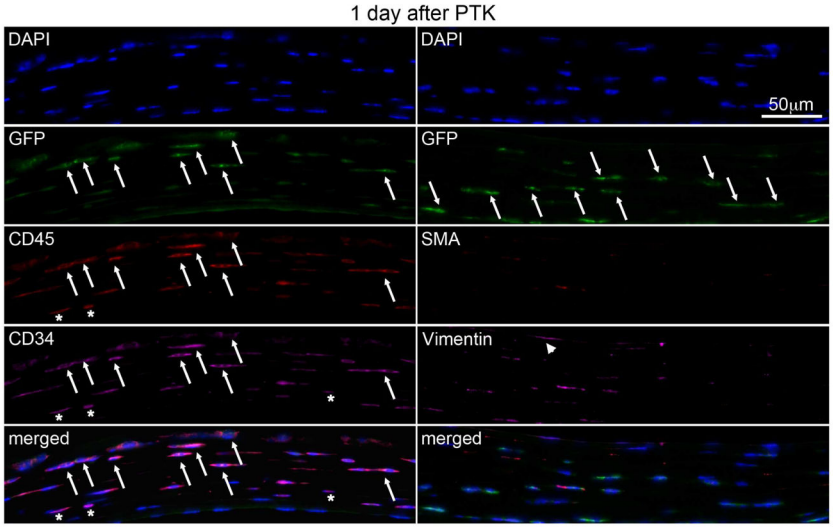

Fig. 3.

Multiplex IHC in chimeric mouse corneas at 1 day after irregular PTK. A large numbers of bone marrow derived GFP+ cells (arrows) were present in corneal stroma. These cells co-express CD45 (arrows) and CD34 (arrows). There were no cells positive for the myofibroblast marker α-SMA. In the merged panel on the bottom left, many GFP+ cells are also CD45+ and CD34+, and likely include fibrocytes (arrows). Some stromal cells are vimentin+ (arrowheads), and these cells also likely include fibrocytes. Asterisks indicate cells that were CD34+ and/or CD45+ that were GFP-. Blue is DAPI staining of cell nuclei. Merged is the overlay of all images in that column. Negative control IHC was performed for all antigens without primary antibody and no staining was detected (not shown). 400x mag.

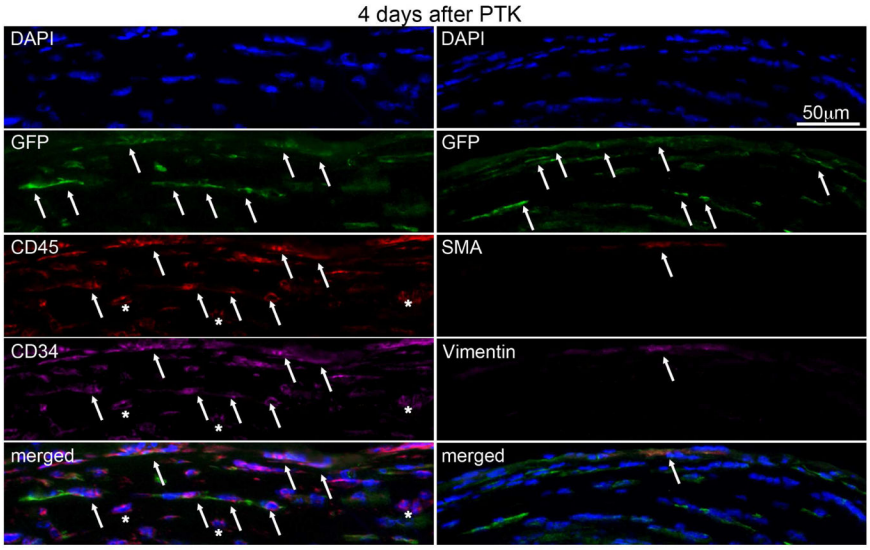

Fig. 4.

Multiplex IHC in chimeric mouse corneas at 4 days after irregular PTK. A large number of bone marrow-derived GFP+ cells (arrows) were present in the stroma. Most of cells were also CD45+ (arrows) and CD34+. The overlay on the bottom left confirms this co-expression (arrows) of GFP, CD45 and CD34 in many cells, and among these cells are fibrocytes. Some cells are GFP+vimentin+ (arrow) indicating fibrocytes or myofibroblasts derived from fibrocytes. Blue is DAPI staining of cell nuclei and merged is the overlap of all images in that column. Negative control IHC was performed for all antigens without primary antibody and no staining was detected (not shown). 400X mag.

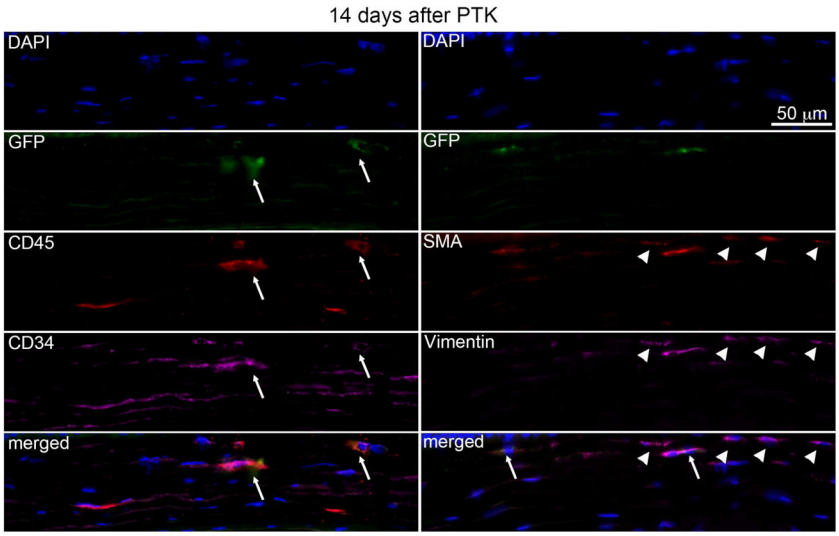

Fig. 5.

Multiplex IHC in chimeric mouse corneas 14 days after irregular PTK. GFP+ (arrows), CD45+ (arrows) and CD34+ (arrows) cells, including those co-expressing all three markers seen in the lower left overlay (arrows), were present in the stroma, but at lower density compared to corneas at 4 days and 7 days after PTK. All GFP+ cells co-expressed vimentin (arrows in overlay bottom right) and some expressed αSMA. Approximately two to three times more αSMA+ myofibroblasts were present in each corneal section of all three corneas compared to 7 days after PTK. Also, 30 to 50% of αSMA+ cells in each corneal section were GFP- (arrowheads, including in the overlay at the bottom right) indicating a keratocyte origin. Blue is DAPI staining of cell nuclei. Negative control IHC was performed for all antigens without primary antibody and no staining was detected (not shown). 400X mag.

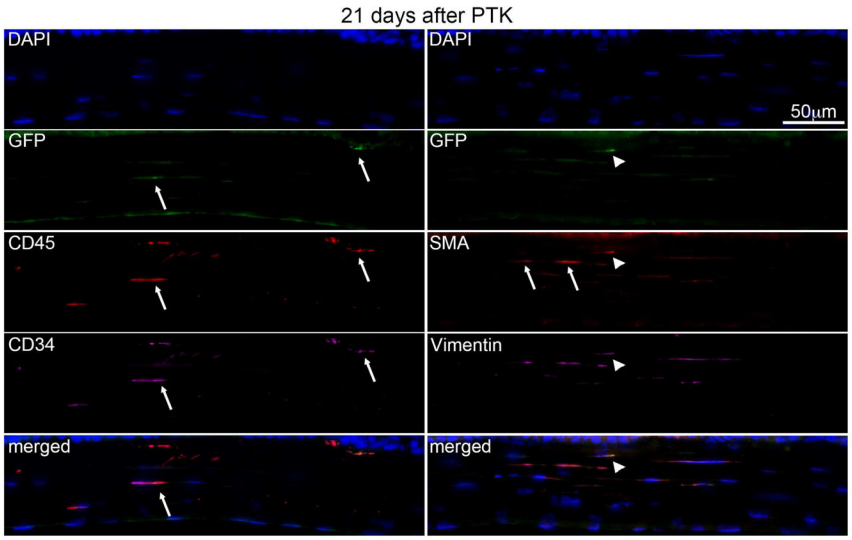

Fig. 6.

Multiplex IHC in chimeric mouse corneas 21 days after irregular PTK. Fewer bone marrow-derived GFP+ cells (arrows) were present in the stroma of all three corneas at 21 days after PTK. The GFP+ cells that were present were also CD45+ (arrow) and CD34+ (arrow), although in some sections there were GFP+CD45+ cells that were CD34- (not shown). The overlay on the bottom left shows the co-expression of GFP, CD45, and CD34 in one cell (arrow). In this section, only one αSMA+ myofibroblast was GFP+ (arrowhead, including in the bottom right overlay) while two αSMA+ myofibroblasts were GFP- (arrows). Blue is DAPI staining of cell nuclei. Negative control IHC was performed for all antigens without primary antibody and no staining was detected (not shown). 400X mag.

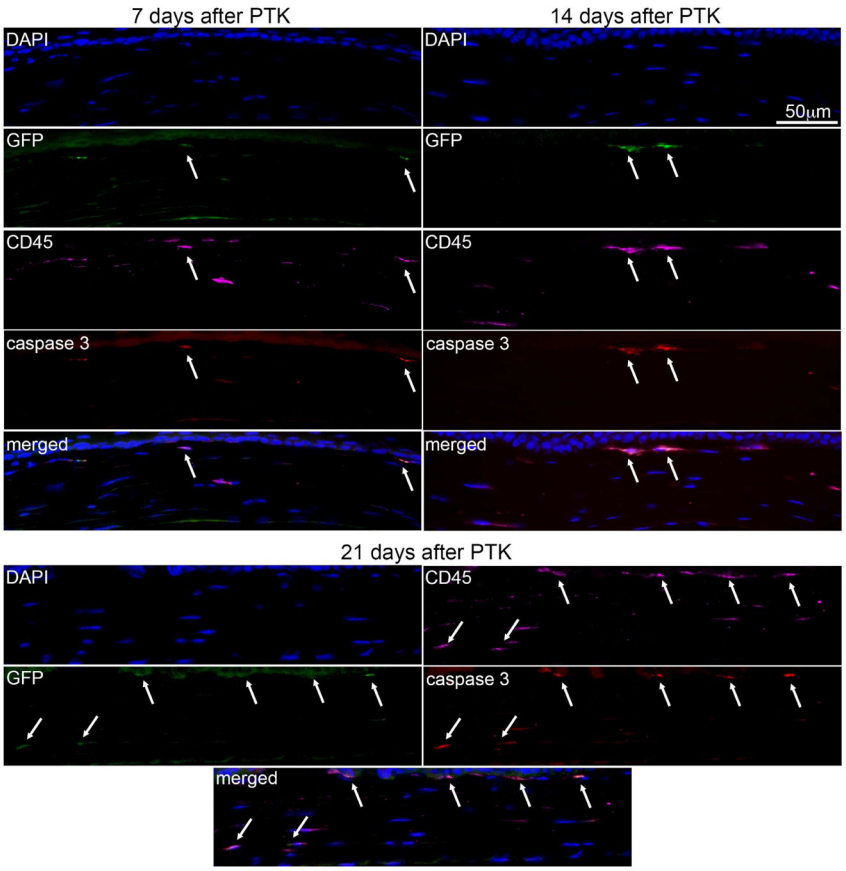

Fig. 7.

Activated cleaved caspase-3, GFP and CD45 multiplex IHC for detection of apoptotic cells in chimeric corneas after irregular PTK. At 7 days, 14 days and 21 days after PTK, two to four activated cleaved caspase-3 expressing cells (arrows) were detected in each section evaluated of all three corneas at each time point. More than 95% of these apoptotic cells were also GFP+ and CD45+, indicating that many invading bone marrow-derived cells, including fibrocytes, undergo apoptosis at some point more than four days after irregular PTK. Blue is DAPI staining of cell nuclei. Negative control IHC was performed for all antigens without primary antibody and no staining was detected (not shown). 400X mag.

Table 1

Averages of marker-positive cells alone and in multiplex combinations per 400X field

	GFP+	CD45+	CD34+	GFP+/CD45+	GFP+/CD34+	GFP+/CD45+/CD34+
Control	0.0±0	3.8±2.2	14.0±1.6	0.0±0	0.0±0	0.0±0
1 day	51.0±5.0	52.5±5.0	53.3±5.0	51.0±5.0	51.0±5.0	51.0±5.0
4 days	67.3±6.4	74.3±6.0	74.7±5.5	67.3±6.4	67.3±6.4	67.3±6.4
7 days	15.7±2.1	18.7±4.6	18.7±4.6	15.7±2.1	15.7±2.1	15.7±2.1
14 days	3.0±1.0	6.0±2.6	14.0±1.0	3.0±1.0	3.0±1.0	3.0±1.0
21 days	2.3±1.2	6.0±2.6	7.3±0.6	2.3±1.2	2.3±1.2	2.3±1.2

	GFP+	αSMA+	CD45+	GFP+/αSMA+	GFP+/CD45+	GFP+/CD45+/αSMA+
Control	0.0±0	0.0±0	4.5±1.3	0.0±0	0.0±0	0.0±0
1 day	47.7±2.1	0.0±0*	53.0±2.0	0.0±0*	47.7±2.1	0.0±0*
4 days	67.0±2.8	1.5±0.7	71.5±3.5	1.5±0.7	67.0±2.8	1.5±0.7
7 days	13.0±1.4	7.0±1.4	16.5±0.7	6.5±0.7	13.0±1.4	6.5±0.7
14 days	3.7±1.5	5.7±1.5	6.0±2.0	3.7±1.5	3.7±1.5	3.7±1.5
21 days	1.3±0.6	2.0±1.0	1.7±1.2	1.3±0.6	1.3±0.6	1.3±0.6

	GFP+	αSMA+	Vimentin+	GFP+/αSMA+	GFP+/Vimentin+	GFP+/Vim+/αSMA+
Control	0.0±0	0.0±0	3.5±0.6	0.0±0	0.0±0	0.0±0
1 day	44.3±3.2	0.0±0*	12.3±2.5	0.0±0*	12.3±2.5	0.5±0.3*
4 days	66.0±1.4	1.0±0.7	8.0±1.4	1.0±0.7	1.0±0.7	1.0±0.7
7 days	12.7±4.2	7.3±0.7	17.0±1.4	7.0±0.3	7.3±0.7	7.0±0.4
14 days	3.3±0.9	5.3±0.9	7.3±0.9	3.3±0.9	3.3±0.9	3.3±0.9
21 days	1.0±0.3	3.0±1.4	4.0±1.4	1.0±0.1	1.0±0.3	1.0±0.2

Averages of cells positive for fibrocyte and myofibroblast markers in different multiplex combinations. Three different immunofluorescence multiplexes were performed per animal at the different time points and quantification for all combinations is presented in the table. All differences were statistically significant compared to the unwounded control group, $p<0.01$, except those indicated by *.

Table 2

Averages of marker-positive cells alone and in different multiplex combinations per 400X field

	GFP+	CD45+	Caspase 3+	GFP/CD45+	CD45/Casp3+	GFP/CD45/Casp3+
Control	0.0±0	5.0±1.2	0.0±0	0.0±0	0.0±0	0.0±0
4 days	39.0±15.5	43.5±16.2	39.0±1.4	2.0±15.6	2.0±1.4	2.0±1.4
7 days	5.5±2.1	6.5±2.1	5.5±2.1	2.5±2.1	2.5±2.1	2.5±2.1
14 days	2.0±0.1	4.0±0.1	2.0±0.0	1.9±0.9	2.0±0.6	2.0±0.0
21 days	3.0±1.4	8.0±2.8	2.0±1.4	3.0±0.2	3.0±1.4	3.0±1.4

Averages of cells positive for hematopoietic and apoptosis markers in different multiplex combinations per 400X microscope field in the stroma. Three different immunofluorescence multiplexes were performed per animal at the different time points and quantification for all combinations is presented in the table. All differences were statistically significant compared to the unwounded control group, $p<0.01$.